AGU Advances

RESEARCH ARTICLE
10.1029/2021AV000546

Decreased Aviation Leads to Increased Ice Crystal Number and a Positive Radiative Effect in Cirrus Clouds

Jialei Zhu[1], Joyce E. Penner[2], Anne Garnier[3], Olivier Boucher[4], Meng Gao[5], Lei Song[6], Junjun Deng[1], Cong-qiang Liu[1], and Pingqing Fu[1]

[1]Institute of Surface-Earth System Science, School of Earth System Science, Tianjin University, Tianjin, China, [2]Department of Climate and Space Sciences and Engineering, University of Michigan-Ann Arbor, Ann Arbor, MI, USA, [3]Science Systems and Applications, Inc., Hampton, VA, USA, [4]Institut Pierre-Simon Laplace, Sorbonne Université/CNRS, Paris, France, [5]Department of Geography, Hong Kong Baptist University, Hong Kong, China, [6]Center for Monsoon System Research, Institute of Atmospheric Physics, Chinese Academy of Sciences, Beijing, China

Key Points:

- A significant increase in the number of ice crystals in cirrus clouds was found due to the decreased aircraft soot emission
- The increased ice crystal number can be explained by an enhancement of homogeneous freezing due to the decreased ice nuclei particles
- Worldwide adoption of biofuel blending could lead to a significant change in the microphysical properties of cirrus clouds in the future

Supporting Information:

Supporting Information may be found in the online version of this article.

Correspondence to:

J. E. Penner and J. Zhu,
penner@umich.edu;
zhujialei@tju.edu.cn

Citation:

Zhu, J., Penner, J. E., Garnier, A., Boucher, O., Gao, M., Song, L., et al. (2022). Decreased aviation leads to increased ice crystal number and a positive radiative effect in cirrus clouds. *AGU Advances*, *3*, e2021AV000546. https://doi.org/10.1029/2021AV000546

Received 3 AUG 2021
Accepted 16 FEB 2022

Peer Review The peer review history for this article is available as a PDF in the Supporting Information.

Author Contributions:

Conceptualization: Jialei Zhu, Joyce E. Penner, Meng Gao
Formal analysis: Jialei Zhu, Anne Garnier, Pingqing Fu
Funding acquisition: Cong-qiang Liu, Pingqing Fu
Investigation: Meng Gao

Abstract Travel restrictions in the wake of the COVID-19 pandemic resulted in an unprecedented decrease of 73% in global flight mileage in April–May 2020 compared to 2019. Here we examine the CALIPSO satellite observations and find a significant increase in ice crystal number concentrations (Ni) in cirrus clouds in the mid-latitudes of the Northern Hemisphere, which we attribute to an increase in homogeneous freezing when soot from aircraft emissions is reduced. A relatively small positive global average radiative effect of 21 mW m^{-2} is estimated if a decrease in aircraft traffic continues, with an average of up to 64 mW m^{-2} over the area where aviation is most active. We infer from this analysis that the worldwide adoption of biofuel blending in aircraft fuels that lead to smaller soot emissions could lead to a significant change in the microphysical properties of cirrus clouds but a rather small positive radiative effect.

Plain Language Summary Cirrus clouds play an important role in the Earth's radiation budget. Whether soot from aircraft emissions would change the property of large-scale cirrus clouds has been a critical question. We show that the unprecedented decrease in aircraft traffic as a result of the COVID-19 pandemic leads to a significant increase in ice crystal number as detected by satellite. An increase in ice crystal number and positive radiative effect is estimated using a state-of-the-science earth system model if the reduction in aviation activity continues for the foreseeable future. As adoption of blending biofuel in the aviation sector would lead to similar reductions (50%–70%) of aircraft soot emissions in the future, remarkable changes in the microphysical properties of large-cirrus clouds and positive radiative effects can be expected relative to a case with no biofuel blending.

1. Introduction

The novel coronavirus disease that started in 2019 (COVID-19) has been spreading worldwide since the end of 2019, which has led to ~250 million infections and ~5 million deaths (Worldometers, 2021). Many countries have taken mandatory lockdown measures, such as closing businesses and factories and encouraging work-from-home, in order to curb the spread of COVID-19. In addition, countries have taken measures to reduce non-essential national and international travel via aircraft in order to reduce the risk of spreading COVID-19 in airports and aircraft cabins as well as to limit the number of cases imported from abroad (Bogoch et al., 2020a, 2020b). Even though social systems and the economy are recovering gradually in some countries where the pandemic is under control, some international borders are still partially or completely closed. As a result, global airlines have been forced to cut flights on a scale that has never been seen before. As many professionals are getting used to remote meetings and online conferences (Bavel et al., 2020), a full recovery of the airline industry may still be expected to take several years despite the ongoing vaccine roll-out on a global scale (Adrienne et al., 2020). The succession of lockdown measures during COVID-19 allows for an unprecedented test of anthropogenic influences on the environment and climate. Many studies have been conducted to examine the side effects of these lockdown measures on air quality, decreases in CO_2 emissions and climate responses, mostly caused by the large reduction in the consumption of fossil fuels in factories, power plants and motor vehicles (Forster et al., 2020; He et al., 2020; Huang et al., 2020; Le Quéré et al., 2020; Phillips et al., 2020; Venter et al., 2020; Yang et al., 2020). However, very few studies have explored the possible effect of aircraft flight reductions on large-scale cirrus clouds, which may also lead to climate change.

Methodology: Jialei Zhu, Joyce E. Penner, Anne Garnier, Olivier Boucher, Lei Song
Project Administration: Cong-qiang Liu, Pingqing Fu
Resources: Joyce E. Penner, Anne Garnier, Olivier Boucher, Lei Song
Supervision: Joyce E. Penner, Cong-qiang Liu, Pingqing Fu
Validation: Jialei Zhu, Junjun Deng
Visualization: Jialei Zhu
Writing – original draft: Jialei Zhu, Joyce E. Penner, Anne Garnier, Olivier Boucher
Writing – review & editing: Jialei Zhu, Joyce E. Penner

Aircraft field experiments have found that aviation exhaust particles may contribute to changes in the number densities and size of ice crystals in cirrus clouds (Ström & Ohlsson, 1998; Urbanek et al., 2018). These changes to ice crystals would impact the ice water path, cloud cover, lifetime, and optical properties of large-scale cirrus clouds and thus determine their radiative properties. Satellite observations suggested a systematic, statistically significant increase in cirrus cloud optical thickness associated with aircraft flight tracks as well as complex changes in ice crystal effective radius in cirrus clouds associated with anthropogenic pollution (Tesche et al., 2016; Zhao et al., 2019).

The ice crystal number concentration (Ni) in cirrus clouds is determined by the competition between homogeneous freezing of haze particles such as sulfate and heterogenous nucleation (i.e., the formation of ice initiated by the contact of liquid or gas phase water with a solid or amorphous particle). Heterogeneous nucleation may take place on ice nucleating particles (INPs) such as aircraft soot and dust particles (Cantrell & Heymsfield, 2005; Koop et al., 2000). Homogeneous freezing occurs when the relative humidity with respect to ice (RHi) is high (of the order of 150%), while heterogeneous nucleation requires much lower RHi (Hoose & Möhler, 2012). As a result, heterogeneous nucleation can occur in advance of homogeneous freezing in a rising air parcel, and thereby consume the limited water vapor supply, suppressing the occurrence of homogeneous freezing. Here we examine the effect of the decrease in aircraft soot emissions on large-scale cirrus clouds using a combination of remote sensing and modeling.

2. Materials and Methods

2.1. Flight Mileage and Aircraft Soot Emissions

The FlightRadar24 commercial database of individual flights for January-May in 2019 and 2020 were used to reconstruct the daily spatial distribution (at $1° \times 1°$ resolution) of air traffic and then interpolated into our model grids (at $1.9° \times 2.5°$ resolution). The aircraft routes were assumed to follow great circles between the start and the end of the cruising parts of their respective flights. We have assessed the difference in the aircraft routes between using the assumption of shortest (i.e., great circle) and fastest (i.e., fuel optimal) routes. For our grid resolution of $1.9° \times 2.5°$ the difference is fairly small and has a negligible effect on the distribution of aviation-emitted soot. The Aviation Environment Design Tool (AEDT) data set was used to calculate aircraft soot emissions for 2006, which were developed based on the original flight tracks of each of 31 million commercial flights worldwide (Barrett et al., 2010; Wilkerson et al., 2010). The annually averaged growth rate of aircraft soot emissions over the period 2006–2012 is 2.2% yr^{-1} and for 2013–2019 is 5% yr^{-1} (Lee et al., 2021). The aircraft soot emission in January–May 2020 was estimated to be the emission in 2019 multiplied by the ratio of flight mileage in each grid for 2020 to that for the same month in 2019. The difference in aircraft soot emission in April/May between 2020 and 2019 is shown in Figure S1 in Supporting Information S1.

2.2. CALIPSO Satellite Observations

Observed Ni are derived from co-located observations of the Imaging Infrared Radiometer (IIR) and the Cloud and Aerosol Lidar with Orthogonal Polarization (CALIOP) lidar aboard the Cloud-Aerosol Lidar and Infrared Pathfinder Satellite Observation (CALIPSO) satellite. The retrieval technique uses the ratio, β_{eff}, of the effective absorption optical depths in IIR channels 12.05 and 10.6 μm and relationships established from SPARTICUS data using the $N(D)_1 = 0$ assumption (Mitchell et al., 2018). The β_{eff} ratios are from the recent Version 4 IIR Level 2 track products (Garnier et al., 2021a, 2021b), which include improvements with respect to the previous Version 3 that were applied in a previous study (Mitchell et al., 2018). Following Version 3, Ni is retrieved for single-layered semi-transparent cirrus clouds with temperature at cloud base altitude colder than 238 K and cloud optical depth larger than about 0.3. The relative uncertainties in Ni retrievals vary with the relative uncertainties in COD, which increase rapidly when COD is small ($COD < 0.3$), so that Ni in clouds with $COD < 0.3$ were not retrieved in this study (Mitchell et al., 2018). Since September 2016, the quality of the CALIOP data over the South Atlantic Anomaly (SAA) region is impacted by an increasing number of low energy laser shots. In order to prevent changes that would result from lower quality data since 2016 over the SAA, this region is removed from all the statistics for the full time period.

2.3. CESM/IMPACT Model

We used the Community Earth System model (CESM) version 1.2.2 (refer to http://www.cesm.ucar.edu/models/cesm1.2 for details) coupled to the University of Michigan IMPACT aerosol model with a resolution of 1.9° (longitude) × 2.5° (latitude) and 30 vertical layers to simulate aerosols and their effects on cirrus clouds. This version of the IMPACT model simulates the number and mass of pure sulfate in three modes (i.e., nucleation (<5 nm), Aitken (5–50 nm) and accumulation (>50 nm)) and their interaction with the following fourteen other aerosol species/types. Sulfate is the only aerosol participating in homogeneous ice nucleation in the model. Soot from fossil fuel and biofuel burning (fSoot) is simulated in three modes with different hygroscopicity according to the number of monolayers of sulfate on its surface while soot from biomass burning (bSoot) is simulated in one mode. 0.05% of fSoot with <1 monolayers of sulfate and 0.1% of fSoot coated with 1–3 monolayers of sulfate as well as 0.1% of bSoot are assumed to be effective INPs. Aircraft soot is simulated in two modes. The first mode has acted as an ice nuclei within contrails that subsequently evaporated (cSoot). The second mode which has not acted as an ice nuclei within contrails has only a small ability to act as an INP compared to the first mode and is not considered to act as an INP in the model. The soot that has already been included in contrail ice is treated as pre-activated. We assume that 100% of the pre-activated aircraft soot coated with less than 3 monolayers of sulfate can be an INP, similar to the treatment in previous studies (Mahrt et al., 2019; Zhou & Penner, 2014) and consistent with field observations of dust and the treatment of dust in the model. This results in approximately 0.6% of all emitted aircraft soot that can possibly acting as an INP to form ice. The model's ability to simulate the profile of soot from fossil fuel, biofuel and aircraft emissions was evaluated by comparison with field campaigns (Figure 2 in Samset et al., 2014; Figure S15 in Zhu & Penner, 2020a). Dust and sea salt are each carried in four separate bins with varying radii. It is assumed that dust with fewer than 3 monolayers of sulfate coating can act as an INP to form ice in the model. As noted in Penner et al. (2018), this treatment is consistent with the results of field studies (Cziczo et al., 2004; P. DeMott et al., 2003; Richardson et al., 2007). The explicit number concentration of newly formed secondary organic aerosol (SOA) in the accumulation mode nucleated from highly oxygenated organic molecules (HOMs) that form from the oxidation of α-pinene is read in as a possible INP in the model. The nucleated SOA particles grow by deposition and coagulation of sulfuric acid as well as by oxidation products of isoprene, α-pinene, limonene and aromatics, that are in the aerosol phase. This SOA was simulated using the version of the CESM/IMPACT model outlined in our previous studies (Zhu & Penner, 2019; Zhu et al., 2017; Zhu et al., 2019). The SOA that meets the requirements of the glass transition temperature and RHi calculated using the equations in Wang et al. (2012) is able to act an effective heterogeneous INP. Soot (i.e., aircraft, fSoot, and bSoot) as well as SOA were set to activate at an RHi of 135% (but with varying fractions, see above) while dust satisfying the sulfate coating criteria activates at 120%. The assumptions for aerosols to be effective INPs in the model are summarized in Table 1 of Penner et al. (2018).

The HYBRID ice nucleation scheme is used to calculate the initial ice crystal number concentration in cirrus clouds from homogeneous and heterogeneous nucleation of aerosols. The HYBRID scheme combines the best features of two previous ice nucleation schemes, so that our model is able to calculate the ice number concentration change in both updrafts and downdrafts associated with a parameterization of sub-grid scale gravity waves and has a robust sensitivity to the change in aerosol number. The effect of ice nucleation within pre-existing ice in cirrus clouds is not considered in this version of model. The uncertainty associated with the assumption of no ice formation in pre-existing ice is discussed in the Supplemental Text S1 in Supporting Information S1. After ice nucleation, the growth and sedimentation as well as evaporation of ice crystals follow the treatment in the CESM. In addition, the changes to cirrus clouds have feedbacks as a result of changes to the radiation budget, temperature, and the formation of warm clouds, as simulated in the CESM model. The ability of CESM/IMPACT and the HYBRID ice nucleation scheme to simulate the ice crystals in cirrus clouds have been evaluated in (Penner et al., 2018; Zhu & Penner, 2020b).

Two cases (EX_S1 and EX_S2) were run to examine the influence of aircraft emissions reductions due to the COVID-19 pandemic in 2020 on cirrus clouds. In these runs, the winds were nudged towards ECMWF reanalysis data using a nudging time of 6 hr for January 2017 to May 2020. The aircraft soot emissions for EX_S1 and EX_S2 are the same for January 2017 to December 2019. The emission for EX_S1 in 2020 is the same as the emission in 2019, while the emission for EX_S2 in 2020 is decreased based on the reduction in aircraft mileage. The effect of the reduction in aircraft emissions due to the COVID-19 pandemic was estimated as the difference between EX_S2 and EX_S1 in 2020. Two cases, EX_L1 and EX_L2, were run to examine the influence of the

assumption of a long-term reduction in aircraft flights, These were run for 6 years with winds nudged toward ECMWF reanalysis data using a nudging time of 6 hr for the years 2009–2014. The data for the last five years were used for analysis. The aircraft emissions in EX_L1 are increased by 5% per year from the emissions in 2019, while the aircraft emissions in EX_L2 are decreased from that in EX_L1 by the ratio of flight mileage reduction in April/May 2020 compared to April/May 2019. The difference in the ice crystal number, Ni, and radiation between EX_L2 and EX_L1 is the long-term effect of the aircraft reductions on cirrus clouds.

3. Results

3.1. Decrease in Global Flight Mileage Due To COVID-19

Global aircraft flight mileage increased by ~5% annually between 2012 and 2019 (based on global aviation fuel use; Lee et al., 2021) due to the rapid expansion of civil aviation (SABRE, 2020). This pattern of growth was expected to continue for the next two decades before the COVID-19 outbreak according to Airbus's global market forecast (Airbus, 2019). However, this trend was terminated when international airlines stopped operating flights into and out of China in February 2020. We reconstructed the daily spatial distribution of air traffic using the FlightRadar24 commercial database of individual flights for 2019 and 2020 (Figure S2 in Supporting Information S1). Flights were reduced in China while fights were still slightly increased in other regions in the early stage of the pandemic (January and February 2020) compared to the same period in 2019, resulting in a 0.3% decrease in global average flight mileage (Figure S2a in Supporting Information S1). Travel restrictions gradually spread over the world in March 2020 with a decrease of 26% in the global average flight mileage compared to March 2019 (Figure S2b in Supporting Information S1). In April and May 2020, flights were reduced significantly all over the world and global average flight mileage was decreased by 73% compared to that for the same period in 2019, which we term the severe stage of the pandemic (Figure S2c in Supporting Information S1). Here we examine the change in cirrus clouds in January-February (relative to previous years) and the change in April-May (relative to previous years).

3.2. Increased Ice Crystal Number Detected by Satellite

Satellite remote sensing provides a unique method for monitoring the global distribution of cloud properties with high spatial resolution, which enables the examination of changes to cirrus clouds and climate during the lockdown period. Figure 1 shows the average and median Ni in four latitude bands (30°N ~ 60°N, 0°N ~ 30°N, 30°S ~ 0, 60°S ~ 30°S) retrieved from CALIPSO observations (details in Section 2.2). Both the median and the average Ni were similar in January-February of 2018, 2019 and 2020. In contrast, it is evident that the median and average Ni in April-May of 2020 is higher relative to Ni for 2018 and 2019 between 30°N ~ 60°N latitude and 22.5°E ~ 97.5°E longitude and Ni continues to be slightly higher to about 165°E, which includes China (Figure 1, dotted black box in Panel B). This is immediately downwind of Western Europe, a region with large decreases in aviation (Figure S2c in Supporting Information S1). Although aviation also decreased in North America (Figure S2c in Supporting Information S1), the change in Ni is not remarkable over and downwind of North America. Mountainous terrain is downwind (east) of Europe while the Atlantic Ocean is east of North America. Examination of global plots of Ni from satellite remote sensing suggests that homogeneous freezing is most active over mountainous regions (Gryspeerdt et al., 2018; Mitchell et al., 2018; Sourdeval et al., 2018) since retrieved Ni is highest over and downwind of these regions. A large eddy simulation (LES) study shows that cirrus Ni in orographic regions changes rapidly as INP concentrations increase above those for a pure homogeneous freezing case (Joos et al., 2014). Thus, the largest changes in Ni in the 30°N ~ 60°N latitude band may be over mountainous terrain downwind of aviation decreases.

Most cirrus clouds in the tropics (between 30°S ~ 30°N) are of convective origin (i.e., anvil cirrus) where ice crystals are nucleated in the strong updraft below the cirrus anvil by either homogeneous or heterogeneous nucleation or ice multiplication processes (P. Lawson et al., 2017; R. P. Lawson et al., 2015), often in a mixed phase environment (Gasparini et al., 2019; Gasparini et al., 2018). This differs greatly from cirrus conditions outside of the tropics especially during non-summer months where homogeneous and heterogeneous nucleation may compete in non-anvil (i.e., large-scale) cirrus. This competition process is much more likely to be sensitive to a change in INPs (Joos et al., 2014). Therefore, due to the different nucleation processes, changes in INP concentration are not as likely to affect cirrus Ni in the latitude band from 30°S ~ 30°N (Figure 1c). The latitude band

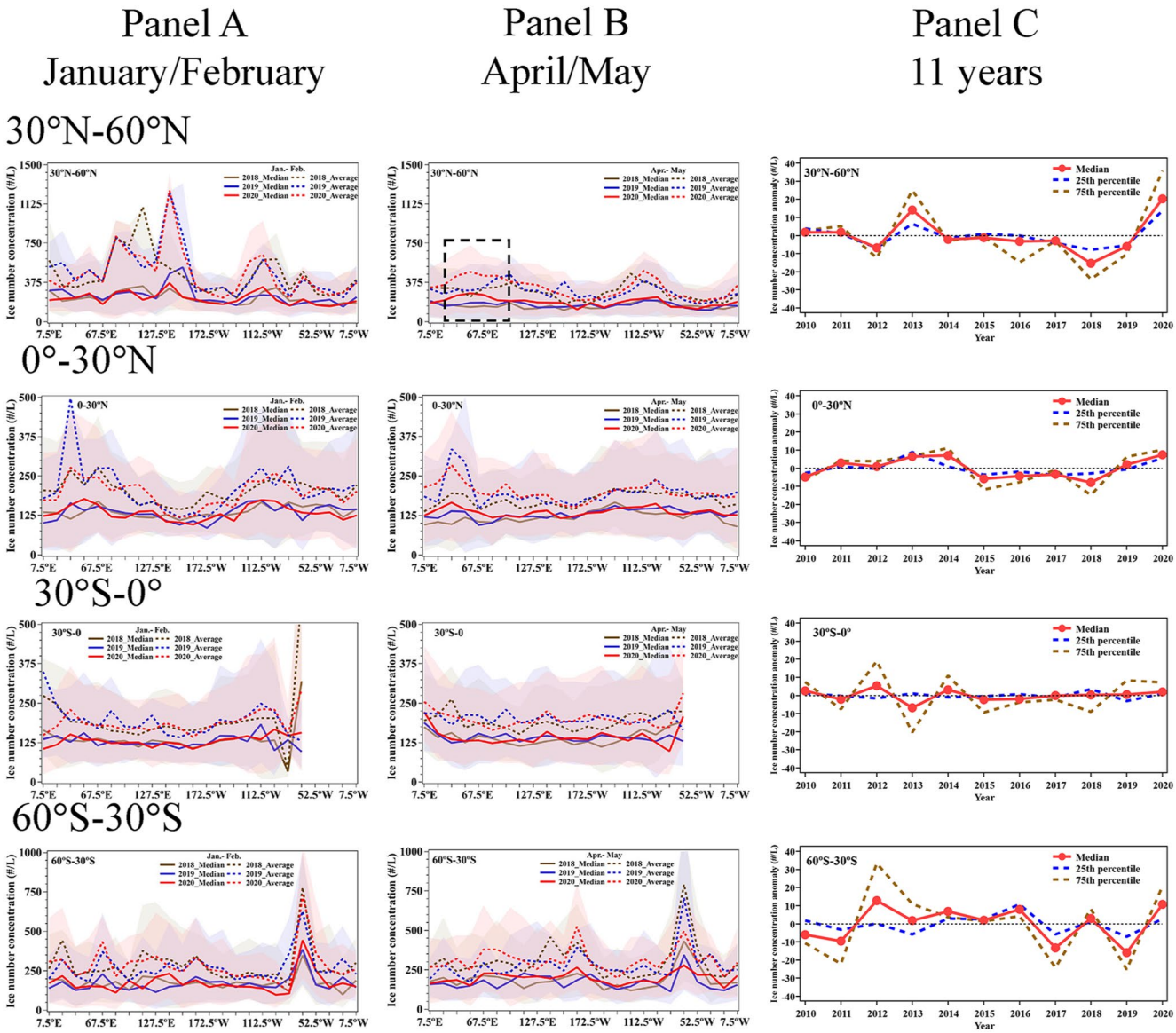

Figure 1. The number concentration of ice crystal (Ni) from CALIPSO observations in the latitude bands of 30°N ~ 60°N, 0°N ~ 30°N, 30°S ~ 0, and 60°S ~ 30°N. Panel (a) the comparison of median and average Ni in January-February between 2018, 2019 and 2020. Panel (b) the comparison of median and average Ni in April-May between 2018, 2019 and 2020. Panel (c) The median as well as 25th and 75th percentile detrended Ni anomaly (L^{-1}) in April and May from 2010 to 2020. The dotted black box indicates a region where Ni in April-May of 2020 is evidently higher relative to Ni for 2018 and 2019.

between 60°S ~ 30°S is also not likely to exhibit significant changes in cirrus Ni since this latitude band experiences relatively little aviation (Figure S2 in Supporting Information S1). The Ni peak at ~70°W in the band from 60°S ~ 30°S is possibly due to orographic ascent over the Andes (Gryspeerdt et al., 2018; Mitchell et al., 2018).

Paired Student's *t* tests (for averages) and Mood's tests (for medians) were applied for the change in Ni in 2020 relative to 2018 and 2019 to examine the significance of changes (Table 1). The differences in the median and average Ni over all latitude bands in January-February between 2018, 2019 and 2020 were not significant at a 90% significance level. Natural variations in meteorological conditions and regular anthropogenic activities between different years within a three-year period thus do not affect large-scale cirrus clouds significantly. However, the change in both the median and average Ni concentrations over 60°S–60°N in April-May 2020 are significantly different from those in 2018, 2019 and the average of 2018 and 2019 at a >95% significance level (Table 1). The median Ni over 30°N–60°N in April-May 2020 was significantly different from that in 2018 and 2019 at a >95% significance level. The difference in the median and average Ni in April–May 2020 was also significant compared

Table 1
Difference in the Median and Average Ni (L^{-1}) Between 2019 and 2018, 2020 and 2019, and 2020 and 2019 as Well as the Difference Between 2020 and the Average of 2019 and 2018 and Between 2020 and the Average of 2010–2019 as Measured by CALIPSO

			2019-2018	2020–2018	2020–2019	2020-AVE1[a]	2020-AVE2[b]
Jan–Feb	Median	60°S–60°N	3.44	−1.59	−5.04	−3.32	-
		30°N–60°N	19.31	−5.37	−24.68	−15.02	-
		0°N–30°N	−2.56	−2.93	−0.38	−1.66	-
		30°S–0°S	0.52	2.72	2.19	2.45	-
		60°S–30°S	−4.00	−0.08	3.92	***1.92***	-
	Average	60°S–60°N	3.26	−2.61	−5.87	−4.24	-
		30°N–60°N	22.68	6.19	−16.49	−5.15	-
		0°N–30°N	7.69	−6.86	−14.55	−10.7	-
		30°S–0°S	−4.45	−9.95	−5.51	−7.73	-
		60°S–30°S	−12.88	0.19	13.08	6.64	-
Apr–May	Median	60°S–60°N	−1.28	13.95	***15.23***	***14.59***	***12.74***
		30°N–60°N	9.70	***36.24***	26.54	***31.39***	***24.21***
		0°N–30°N	9.93	15.55	5.61	10.58	***9.07***
		30°S-0°S	−7.03	−4.60	2.43	−1.09	4.69
		60°S–30°S	−18.89	7.85	26.74	17.30	***11.63***
	Average	60°S–60°N	3.00	***20.01***	***17.01***	***18.51***	***14.34***
		30°N–60°N	7.45	***42.15***	***34.71***	***38.43***	***29.68***
		0°N–30°N	***22.06***	***25.41***	3.35	***14.38***	***12.06***
		30°S–0°S	40.43	40.45	0.01	4.19	6.56
		60°S–30°S	−24.45	5.53	29.98	17.76	7.75

Note. Italicized and bold numbers are statistically significant at the 95% level according to a Student's *t* test for the averages and a Mood's test for the medians.
[a]AVE1 stands for the average of Ni in 2018 and 2019. [b]AVE2 stands for the average of Ni from 2010 to 2019.

to Ni in 2018 and the average of 2018 and 2019 over the 0°–30°N latitude band at a >95% significance level. In the Southern Hemisphere (SH), only the median Ni over 60°S–30°S in April–May 2020 is significantly different from that in 2019 and the average in 2018 and 2019.

The median and average Ni in April-May 2020 were also compared to that in April-May over the last 10 years (2010–2019). The Ni concentrations over 60°S–60°N, especially in the Northern Hemisphere (NH), in April–May 2020 were also significantly different from that in the last 10 years at a >95% significance level (Table 1). The Ni anomaly over 30°N ~ 60°N in April–May 2020 stands out from the series of Ni anomalies (after detrending) over 2010–2020 (Figure 1, Panel C). The anomaly in 2013 is nearly as large as that in 2020 (14/L as opposed to 20/L). However, the increase in 2013 may be associated with the unusually cold temperatures in the upper troposphere over 30°N–60°N in April/May 2013, while the average temperature in April/May 2020 was 0.53°C higher than in April/May 2013 (Figure S3 in Supporting Information S1). While meteorological differences cannot be entirely excluded as an explanation for the differences in April-May 2020, the large latitude bands considered here argues against this explanation for 2020 compared to an analysis that only examined the conditions over Europe for contrail formation in 2020 (Schumann et al., 2021). The Ni anomaly in April-May 2020 over other latitude bands was not evidently different from that over the last 10 years (Figure 1, Panel C). In addition, the most evident increases in the observed Ni over 30°N–60°N were found over 30°E−75°E (downwind of western Europe) and 105°E−135°E (over and downwind of Asia) according to the detrended anomalies in Ni in April-May of 2010–2020 (Figure S4 in Supporting Information S1). As shown in Figure S2c in Supporting Information S1, travel restrictions caused the largest reduction of flight mileage in the NH, especially over North America, Europe, and East and Southeast Asia, while there are much smaller influences in the SH. This may

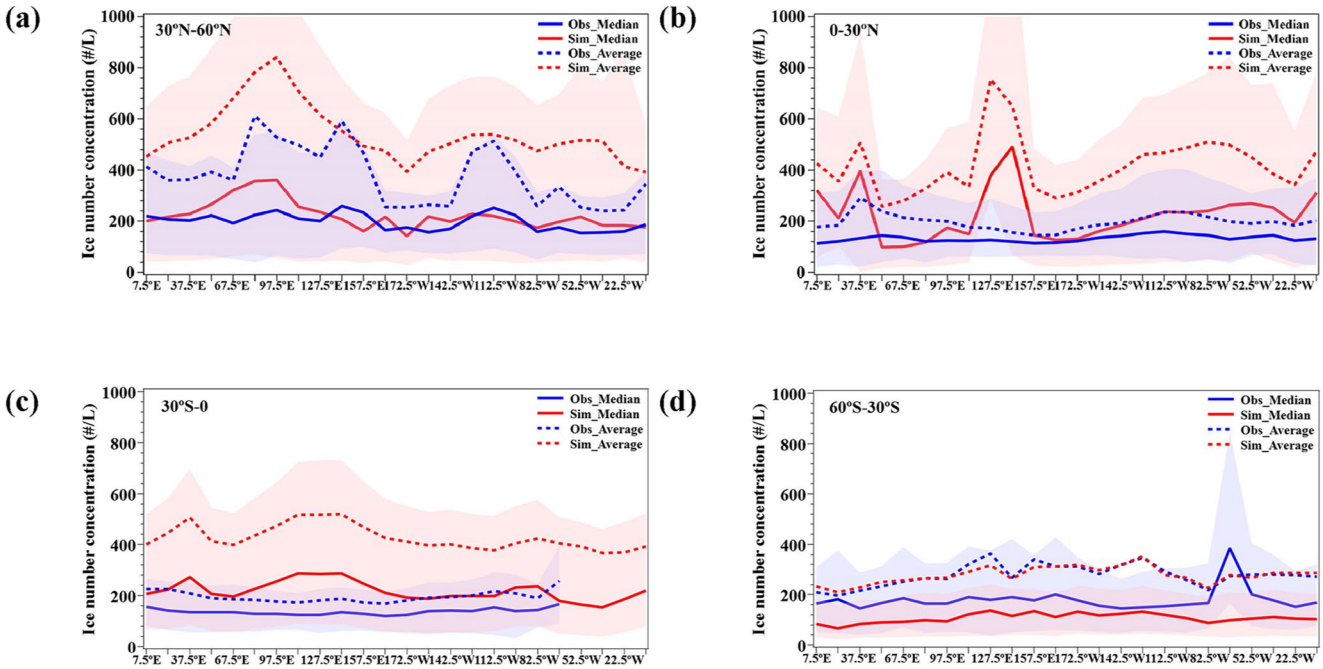

Figure 2. The comparison between observed (blue line) and simulated (red line) median (solid line) and average (dashed line) ice number concentration (L^{-1}) in cirrus clouds for 30°N ~ 60°N (a), 0 ~ 30°N (b), 30°S ~ 0 (c), and 60°S ~ 30°S (d) during January-May from 2018 to 2020. The shading represents the 25th and 75th percentiles of the median.

explain the significant change in Ni from CALIPSO observations over the NH but insignificant change over the SH in April-May 2020 compared to the observed Ni in previous years.

3.3. Microphysical Effects During the Severe Stage of COVID-19

We employed model simulations to attribute the observed changes in Ni to the reduction in air traffic and to determine the effects on cirrus clouds and radiation. The surface emissions of SO_2 and black carbon in China, one of the largest emission sources over the world, were only reduced by 3 ~ 5% in April/May 2020 compared to those in the same months of 2019 (Zheng et al., 2021) while surface emissions of black carbon in Europe decreased by about 11% for January–April (Evangeliou et al., 2021). Since these emissions have a smaller efficiency for the nucleation of new ice crystals in cirrus clouds than do aircraft emissions (Section 2.3) and the reductions of these emissions are smaller than that for aircraft, we assumed that any changes in surface emissions of SO_2 and soot during the pandemic would have a negligible effect on cirrus clouds compared to the large changes in aircraft emissions.

The simulated Ni from January to May in 2018, 2019 and 2020 using the CESM/IMPACT model was evaluated using data from the CALIPSO satellite (Figure 2). The observational data is limited to ice water mixing ratios $>10^{-6}$ kg/kg and cloud optical depths (COD) between 0.3 and 3, so model results are restricted to only these values. When the microphysical index of the infrared imaging radiometer onboard CALIPSO is less than the sensitivity limit for measuring large crystals, Ni was assigned to the values corresponding to this sensitivity limit. As a result, the average Ni determined from CALIPSO was thought to be overestimated (see below, however). It is anticipated that the median Ni is more accurate and can be used to evaluate the model. As shown in Figure 2, the simulated median Ni was close to the observed Ni with an average bias of 21%, and was mostly within the range of the 25th and 75th percentiles of the observations. In contrast, the simulated average Ni is larger than the observed average with an overall bias of 60%. Moreover, the 75th percentile of the simulated Ni is higher than that of the observed Ni. In the model as well as observations, there are infrequent occasions during which very high Ni occur as a result of high updraft velocities and/or smaller INP concentrations (Jensen et al., 2013; Penner et al., 2018). This may indicate that while the model reproduces the median Ni from CALIPSO reasonably well, there are a sufficient number of cases with very high simulated Ni that may be missed by the CALIPSO

observations, thereby reducing the average CALIPSO Ni. It is likely that these are cases in which the crystals are formed by homogeneous freezing. Because the number of aerosol particles that can freeze homogeneously is much larger than the number of INPs, homogeneous freezing always leads to a much higher Ni with smaller ice crystal sizes than cases with significant heterogeneous nucleation. We infer that the CALIPSO average Ni is too low by examining the model results using CALIPSO constraints versus conditions for the model as a whole, as follows. The average Ni for the cases when homogeneous freezing occurs in the model (when constrained to the CALIPSO sampling conditions) is 4042 L^{-1}, which is almost two orders of magnitude larger than the average Ni from heterogeneous nucleation (85 L^{-1}). However, the occurrence frequency of homogeneous freezing is much lower than that of heterogeneous nucleation because of the requirement of higher supersaturations which are typically associated with larger updraft velocities. The annual average occurrence frequency of homogeneous freezing is low for the average of all cases in the model, that is, <15% over different regions with a global average of 2.2% (Figure S5a in Supporting Information S1). However, the occurrence frequency is even lower when the model results are constrained to the COD and ice water mixing ratios for the CALIPSO sampling conditions, that is, a global average of 0.4% with <7% over different regions (Figure S5b in Supporting Information S1). In addition, CALIPSO is a polar orbiting satellite which follows a sun-synchronous orbit. All the CALIPSO satellite observations were made around 0130 and 1330 local time with an average revisit period of ∼16 days. As a result of both the CALIPSO sampling conditions and its polar orbit, CALIPSO may miss the small number of occurrences of homogeneous freezing with high levels of Ni. Consequently, we suggest that the median Ni from CALIPSO should be used to describe the observed Ni, since this would not be as influenced as much as the average Ni as a result of CALIPSO missing some cases when homogeneous freezing occurs. Of course, our radiative forcing estimates (see below) are more sensitive to the average Ni, so these estimates cannot be evaluated using the CALIPSO observations and remain uncertain. When the CALIPSO satellite happens to see a case with homogeneous freezing, the average Ni could be significantly increased. For example, the average Ni near 37.5°E for 0–30°N in January-February of 2019 is larger than the 75th percentile value of the median, possibly because of the influence of homogeneous freezing (Figure 1). Moreover, the CALIPSO satellite has a relatively larger chance of catching the occurrence of homogeneous freezing in polar regions (Figure S5b in Supporting Information S1) because of the constraints used in the CALIPSO algorithm. This might explain the increasing number of pixels with high median Ni in the observations toward polar regions (Figure S6 and Figure 12a in ref Mitchell et al., 2018). In spite of the low occurrence frequency of homogeneous freezing, the high Ni with small ice crystal size caused by homogeneous freezing always dominates the annual average radiative effect of cirrus clouds. Therefore, the CALIPSO satellite observation cannot, by itself, be used to examine the radiative effect of cirrus clouds influenced by changes in aircraft flights. Rather, modeling of ice nucleation and cirrus clouds is needed.

We examined the effect of a decrease in aircraft flights on Ni by contrasting a simulation using the actual aviation activity in 2020 with a second simulation that assumes the same aviation activity in 2020 as in 2019. We decreased the emission of aircraft soot from 2019 to 2020 by the ratio of the flight mileage in 2020 to that in 2019 in each grid. This leads to a decrease of $0.28 \pm 0.44 \times 10^8$ m^{-2} in the modeled global average vertically integrated INPs (i.e., contrail-processed soot with less than 3 monolayers of sulfate) from aircraft soot during April–May 2020 (Figure S7 in Supporting Information S1). As a result, the global average vertically integrated Ni during April-May 2020 was increased by $0.30 \pm 0.68 \times 10^8$ m^{-2} (Figure S8a in Supporting Information S1), while the median vertically integrated Ni increased by $0.06 \pm 0.86 \times 10^8$ m^{-2}. The increase in the average Ni is mostly attributed to the increase of $0.33 \pm 0.68 \times 10^8$ m^{-2} in the contribution of homogeneous freezing, although the Ni from heterogeneous nucleation was decreased by $0.03 \pm 0.26 \times 10^8$ m^{-2} (Figure S8 in Supporting Information S1). The reduction of aircraft soot emissions imposes the largest effect on Ni in the tropics, especially in the western Pacific Ocean and north Indian Ocean, because of the high occurrence frequency of homogeneous freezing there (Figure S5a in Supporting Information S1). Because the change in Ni has a very large standard deviation indicating that this change is not statistically significant in most regions, the radiative effects are also not statistically significant (not shown). Thus, the reduction in aviation flights over a short period such as experienced in April and May 2020, probably does not have a large influence on global climate change, but it offers insights into cirrus processes.

To examine the model's ability to determine the change in Ni, Table S1 in Supporting Information S1 presents the calculated median change in Ni in the model when restricted to the CALIPSO conditions for the same latitude bands and cases as those shown for CALIPSO in Table 1. While most of the calculated changes in Ni for the model are not statistically significant, the difference in the median value for 30–60 N between 2020 and the

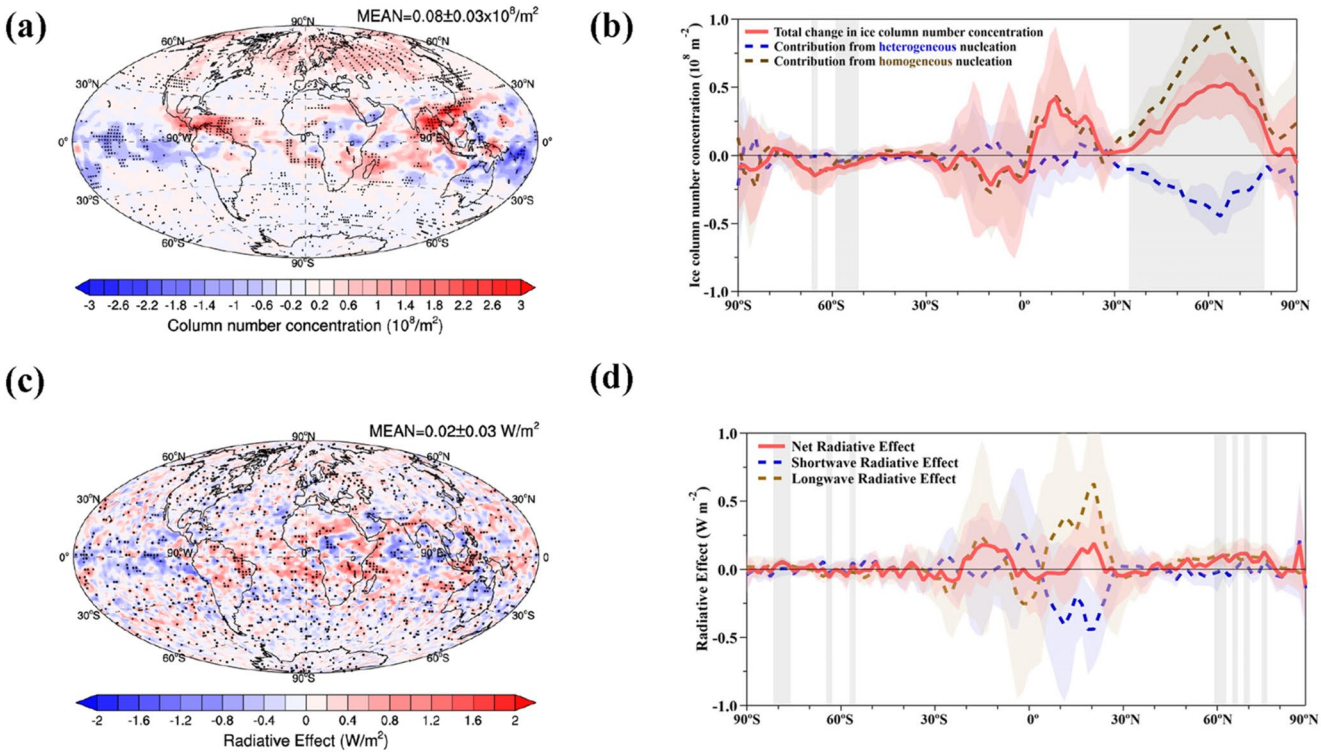

Figure 3. The change in the annual average vertically integrated number concentration (m^{-2}) of total ice crystals (a) and all-sky net radiative effect (W m^{-2}) (c) due to a flight decrease for 5 years. Differences significant at the 95% level according to a Student's *t* test in (a) and (c) are depicted by points. The change in the annual average vertically integrated number concentration of total ice (b, red solid line), ice from homogenous freezing (b, orange dashed line), and ice from heterogeneous freezing (b, blue dashed line) versus latitude due to the reduction in aircraft flights for 5 years. The change in all-sky longwave radiative effect (d, orange dashed line), all-sky shortwave radiative effect (d, blue dashed line), and all-sky net radiative effect (d, solid red line) versus latitude due to a reduction in aircraft flights for 5 years. All plots are the difference between cases EX_L2 and EX_L1 (See methods section). The shading in (b) and (d) represents 1 standard deviation of the interannual variation of the column number concentration and net radiative effect, respectively, over 5 years. Significant differences between (b) and (d) and the 95% level according to a Student's *t* test are depicted by gray shading.

average of 2018 and 2019 is 19 L^{-1} while it was larger for CALIPSO (31 L^{-1}). For 0–30 N the model differences are larger than the observations (16 L^{-1} vs. 11 L^{-1}). It is difficult to draw conclusions from this comparison since the simulated model changes are not significant.

3.4. Radiative Effects of Longer-Term Reductions in Aviation

Given the uncertainty in the duration of the pandemic as well as the uncertainty in vaccine adoption, it is very possible that a reduction in aviation activity could continue for the foreseeable future. As a thought experiment, we assumed that a reduction of aviation activity lasts for five years with the same reduction ratio of aircraft soot emissions as during April-May 2020, thereby exploring the largest possible effect on large-scale cirrus clouds compared to the scenario without any pandemic. This reduction (~73%) in aircraft soot emissions is similar to the anticipated 50 ~ 70% reduction as a result of the blending of biofuels with aircraft kerosene (Moore et al., 2017). In this scenario, the annual global average column number concentration of ice crystals is increased by $0.08 \pm 0.03 \times 10^8$ m^{-2} (Figure 3a). In particular, the increase in Ni is significant over 35°N ~ 75°N in northern Eurasia and over the northern most Atlantic Ocean where air routes are frequent (Figures 3a and 3b). The influence of the flight reduction on Ni in the tropics results in a significant increase in Ni in the north Indian Ocean, Southeast Asia, and the Caribbean Sea together with significant decreases in some regions of the tropical Pacific Ocean (Figure 3a). The larger increases in Ni in the tropics near Asia compared to the changes in mid-latitudes of the NH are the result of the very high levels of homogeneous freezing there (Figure S5 in Supporting Information S1, and Figure 2 in ref (Zhu & Penner, 2020b)), causing larger increases in Ni when the INPs from aircraft are reduced. The decreases in Ni in some parts of the tropical Pacific appear to be associated with a decrease in homogeneous freezing and a small increase in heterogeneous nucleation (Figure 3b) which is thought

to be the result of feedbacks caused by temperature changes associated with the changes in Ni, although more work is needed to confirm this (Zhu & Penner, 2020b). The increase in Ni in the northern mid-latitudes is mostly explained by the significant increase of homogeneous freezing, although the column number concentration of ice crystals from heterogeneous nucleation is decreased due to the decrease in INPs from aircraft soot (Figure S9 in Supporting Information S1). The decrease in INPs weakens the suppression effect of heterogeneous nucleation on homogeneous freezing leading to a significant increase in the occurrence frequency of homogeneous freezing (Figure S10 in Supporting Information S1). This results in an increase of $0.14 \pm 0.04 \times 10^8$ m^{-2} in the global average column number concentration of ice crystals from homogeneous freezing (Figure S9 in Supporting Information S1). The increase in Ni has a positive effect (63 ± 17 mW m^{-2}) on longwave radiation and a negative effect (-41 ± 21 mW m^{-2}) on shortwave radiation (Figure 3d and Figure S11 in Supporting Information S1). As a result, the global annual average net radiation is increased by 21 ± 27 mW m^{-2}, with a particularly significant increase of 64 mW m^{-2} over 50°N ~ 75°N (Figures 3c and 3d). We note that the radiative effect of decreased aviation is sensitive to the concentration of other INPs (e.g., SOA as well as dust and the concentration of sulfate (Zhou & Penner, 2014)). Of these, we consider our treatment of SOA as an INP the most uncertain. If SOA is not included as an efficient INP, the global annual average net radiative effect of a long-term decrease in aviation increases to 34 ± 27 mW m^{-2}, which is 62% more positive than the case reported above that included SOA as an INP (Figure S12 in Supporting Information S1). Moreover, the increase in average ice crystal number due to the decrease in aviation in the case excluding SOA is 19% larger than that in the case that includes SOA. In addition, excluding SOA as an INP leads to an average bias of the median Ni in comparison to CALIPSO of 37% compared to only 21% when SOA is included.

4. Discussion

This study examines the radiative effect of the decrease in aircraft flights due to the COVID-19 pandemic and the resulting increase of Ni in large-scale cirrus clouds in the NH using a combination of remote sensing and modeling. The CALIPSO satellite data indicates that there was a significant increase in Ni in April-May 2020 over 30°N ~ 60°N compared to previous years. The model predicted median Ni is within 21% of that measured by CALIPSO, but because CALIPSO probably misses some homogeneous freezing cases with high Ni, due to the low frequency of homogeneous freezing and long revisit period of CALIPSO, the resulting average Ni is smaller than that in the model. A set of polar orbiting satellites with a higher temporal resolution or a geostationary satellite would be needed in the future to detect average changes in Ni and to examine the cases with homogeneous freezing.

Our model results suggest a significant increase in Ni and a positive radiative effect over most regions in the middle to high latitudes of the NH if flight restrictions last for 5 years. While recent theoretical treatments indicate that the INP efficiency of aircraft soot is quite small (Kärcher et al., 2021), it is not yet clear that such treatments apply to aircraft soot in the atmosphere and its effect on large-scale cirrus clouds. Had we applied such small efficiencies in the model, we would no longer fit the CALIPSO data as well as we do. It might be that the laboratory observations on which Kärcher et al. (2021) based their parameterization do not correctly represent the effects of aircraft soot on large-scale cirrus. Thus, the INP efficiency of aircraft soot that has been incorporated in contrails is possibly the dominant uncertainty in the evaluation of the effect of aircraft emissions on cirrus clouds (P. J. DeMott et al., 1999; Hoose & Möhler, 2012; Mahrt et al., 2020; Mohler et al., 2005). More targeted field measurements are needed in the future to confirm the ability of aircraft soot to act as an INP in different atmospheric conditions and as a result of contrail-processing and coating with other compounds, in order to guide the development of model parametrizations. CALIPSO observations during the flight restriction period associated with the COVID-19 pandemic verifies to some extent the effect of aircraft soot on large-scale cirrus clouds, although it is unable to determine their radiative effects. More measurements of the aircraft soot emission rate and the efficiency of aircraft soot as an INP under various conditions would be useful in the future to better constrain the aircraft soot emission inventory and its radiative effects in the model.

Other uncertainties in the model concern the effect of coatings on INP. We note that the coating on aircraft soot by SOA could alter its ability to act as an INP, and thereby change its effect on cirrus clouds. While sulfuric acid coating decreases the ability of aircraft soot to act as an INP in the model, it is possible that coating by SOA increases its ability. The potential influence of both sulfuric and SOA coating of aircraft soot is discussed more

in the Text S2 in Supporting Information S1, but it is still difficult to quantify the effect of these coatings on ice nucleation. Further quantitative experiments are needed to develop an appropriate parameterization.

While our model does a reasonable job of explaining the increase in Ni in CALIPSO observations, other model choices might also explain this increase. In particular, aircraft contrails are known to increase cirrus clouds and, had we included the effect of pre-existing ice in the model, reductions in aircraft contrails might also increase Ni. However, an examination of high cloud fraction observed by MODIS in April and May 2020 compared to earlier years found only very small changes that were not significant (Table S2 in Supporting Information S1). These small changes in high cloud fraction may be the result of the change in natural cirrus clouds which would increase when contrails are removed (Bickel et al., 2020). Thus it seems that while a decrease in cloud fraction as an explanation for the increase in Ni observed by CALIPSO may be partly responsible, it may be less important than changes in Ni resulting from the decrease in aircraft soot.

Partial or total decarbonization of the aviation sector through blending biofuels with aviation kerosene could reduce the particle number and mass emissions by 50%–70% in the future (Moore et al., 2017). This reduction is comparable to the reduction during the COVID-19 pandemic. Our study would suggest that the adoption of more sustainable fuels, such as biofuel or other synthetic fuels, in the future will increase Ni and change the microphysical properties of cirrus clouds significantly but may only lead to a small positive global average radiative effect. Our radiative forcing calculations for the effects of biofuel adoption on cirrus clouds are only indicative of these possible effects, and are based on estimates of the decrease in aircraft soot emissions together with the model estimates of the effects of these changes on Ni. The net climate effect of biofuel blending or decreased aviation would depend on the effect of all aspects (e.g., CO_2 emissions decrease), which are still uncertain (Lee et al., 2021).

Conflict of Interest

The authors declare no conflicts of interest relevant to this study.

Data Availability Statement

The updated CESM/IMPACT model and model results used in this paper are archived online at http://doi.org/10.5281/zenodo.5154535.

Acknowledgments
This study was supported by the National Natural Science Foundation of China (Grant No. 42177082).

References

Adrienne, N., Budd, L., & Ison, S. (2020). Grounded aircraft: An airfield operations perspective of the challenges of resuming flights post COVID. *Journal of Air Transport Management*, *89*, 101921. https://doi.org/10.1016/j.jairtraman.2020.101921

Airbus (2019). *Global market forecase: Cities, airports & aircraft 2019-2038*. Retrieved from https://www.airbus.com/content/dam/corporate-topics/strategy/global-market-forecast/GMF-2019-2038-Airbus-Commercial-Aircraft-book.pdf

Barrett, S., Prather, M., Penner, J., Selkirk, H., Balasubramanian, S., Dopelheuer, A., et al. (2010). Guidance on the use of AEDT gridded aircraft emissions in atmospheric models. In *A technical note submitted to the US Federal Aviation Administration*. Massachusetts Institute of Technology (MIT).

Bavel, J. J. V., Baicker, K., Boggio, P. S., Capraro, V., Cichocka, A., Cikara, M., et al. (2020). Using social and behavioural science to support COVID-19 pandemic response. *Nature Human Behaviour*, *4*(5), 460–471. Retrieved from https://www.ncbi.nlm.nih.gov/pubmed/32355299

Bickel, M., Ponater, M., Bock, L., Burkhardt, U., & Reineke, S. (2020). Estimating the effective radiative forcing of contrail cirrus. *Journal of Climate*, *33*(5), 1991–2005. https://doi.org/10.1175/jcli-d-19-0467.1

Bogoch, I. I., Watts, A., Thomas-Bachli, A., Huber, C., Kraemer, M. U. G., & Khan, K. (2020a). Pneumonia of unknown aetiology in Wuhan, China: Potential for international spread via commercial air travel. *Journal of Travel Medicine*, *27*(2). https://doi.org/10.1093/jtm/taaa008

Bogoch, I. I., Watts, A., Thomas-Bachli, A., Huber, C., Kraemer, M. U. G., & Khan, K. (2020b). Potential for global spread of a novel coronavirus from China. *Journal of Travel Medicine*, *27*(2). https://doi.org/10.1093/jtm/taaa011

Cantrell, W., & Heymsfield, A. (2005). Production of ice in tropospheric clouds: A review. *Bulletin of the American Meteorological Society*, *86*(6), 795–808. https://doi.org/10.1175/bams-86-6-795

Cziczo, D. J., Murphy, D. M., Hudson, P. K., & Thomson, D. S. (2004). Single particle measurements of the chemical composition of cirrus ice residue during CRYSTAL-FACE. *Journal of Geophysical Research: Atmospheres*, *109*(D4). https://doi.org/10.1029/2003jd004032

DeMott, P., Cziczo, D., Prenni, A., Murphy, D., Kreidenweis, S., Thomson, D., et al. (2003). Measurements of the concentration and composition of nuclei for cirrus formation. *Proceedings of the National Academy of Sciences*, *100*(25), 14655–14660. https://doi.org/10.1073/pnas.2532677100

DeMott, P. J., Chen, Y., Kreidenweis, S. M., Rogers, D. C., & Sherman, D. E. (1999). Ice formation by black carbon particles. *Geophysical Research Letters*, *26*(16), 2429–2432.

Evangeliou, N., Platt, S. M., Eckhardt, S., Lund Myhre, C., Laj, P., Alados-Arboledas, L., et al. (2021). Changes in black carbon emissions over Europe due to COVID-19 lockdowns. *Atmospheric Chemistry and Physics*, *21*(4), 2675–2692. https://doi.org/10.5194/acp-21-2675-5722021

Forster, P. M., Forster, H. I., Evans, M. J., Gidden, M. J., Jones, C. D., Keller, C. A., et al. (2020). Current and future global climate impacts resulting from COVID-19. *Nature Climate Change*, *10*(10), 913–919. https://doi.org/10.1038/s41558-020-0883-0

Garnier, A., Pelon, J., Pascal, N., Vaughan, M. A., Dubuisson, P., Yang, P., & Mitchell, D. L. (2021a). Version 4 CALIPSO Imaging Infrared Radiometer ice and liquid water cloud microphysical properties – Part I: The retrieval algorithms. *Atmospheric Measurement Techniques*, *14*, 3253–3276. https://doi.org/10.5194/amt-14-3253-2021

Garnier, A., Pelon, J., Pascal, N., Vaughan, M. A., Dubuisson, P., Yang, P., & Mitchell, D. L. (2021b). Version 4 CALIPSO Imaging Infrared Radiometer ice and liquid water cloud microphysical properties – Part II: Results over oceans. *Atmospheric Measurement Techniques*, *14*, 3277–3299. https://doi.org/10.5194/amt-14-3277-2021

Gasparini, B., Blossey, P. N., Hartmann, D. L., Lin, G., & Fan, J. (2019). What drives the life cycle of tropical anvil clouds? *Journal of Advances in Modeling Earth Systems*, *11*(8), 2586–2605.

Gasparini, B., Meyer, A., Neubauer, D., Munch, S., & Lohmann, U. (2018). Cirrus cloud properties as seen by the CALIPSO satellite and ECHAM-HAM global climate model. *Journal of Climate*, *31*(5), 1983–2003.

Gryspeerdt, E., Sourdeval, O., Quaas, J., Delanoe, J., Kraemer, M., & Kuehne, P. (2018). Ice crystal number concentration estimates from lidar-radar satellite remote sensing – Part 2: Controls on the ice crystal number concentration. *Atmospheric Chemistry and Physics*, *18*(19), 14351–14370.

He, G., Pan, Y., & Tanaka, T. (2020). The short-term impacts of COVID-19 lockdown on urban air pollution in China. *Nature Sustainability*, *3*(12), 1005–1011. https://doi.org/10.1038/s41893-020-0581-y

Hoose, C., & Möhler, O. (2012). Heterogeneous ice nucleation on atmospheric aerosols: A review of results from laboratory experiments. *Atmospheric Chemistry and Physics*, *12*(20), 9817–9854. https://doi.org/10.5194/acp-12-9817-2012

Huang, X., Ding, A., Gao, J., Zheng, B., Zhou, D., Qi, X., et al. (2020). Enhanced secondary pollution offset reduction of primary emissions during COVID-19 lockdown in China. *National Science Review*. https://doi.org/10.1093/nsr/nwaa137

Jensen, E. J., Lawson, R. P., Bergman, J. W., Pfister, L., Bui, T. P., & Schmitt, C. G. (2013). Physical processes controlling ice concentrations in synoptically forced, midlatitude cirrus. *Journal of Geophysical Research: Atmospheres*, *118*(11), 5348–5360.

Joos, H., Spichtinger, P., Reutter, P., & Fusina, F. (2014). Influence of heterogeneous freezing on the microphysical and radiative properties of orographic cirrus clouds. *Atmospheric Chemistry and Physics*, *14*(13), 6835–6852.

Kärcher, B., Mahrt, F., & Marcolli, C. (2021). Process-oriented analysis of aircraft soot-cirrus interactions constrains the climate impact of aviation. *Communications Earth & Environment*, *2*(1), 113. https://doi.org/10.1038/s43247-021-00175-x

Koop, T., Luo, B. P., Tsias, A., & Peter, T. (2000). Water activity as the determinant for homogeneous ice nucleation in aqueous solutions. *Nature*, *406*(6796), 611–614.

Lawson, P., Gurganus, C., Woods, S., & Bruintjes, R. (2017). Aircraft observations of cumulus microphysics ranging from the tropics to midlatitudes: Implications for a "new'' secondary ice process. *Journal of the Atmospheric Sciences*, *74*(9), 2899–2920.

Lawson, R. P., Woods, S., & Morrison, H. (2015). The microphysics of ice and precipitation development in tropical cumulus clouds. *Journal of the Atmospheric Sciences*, *72*(6), 2429–2445.

Lee, D. S., Fahey, D. W., Skowron, A., Allen, M. R., Burkhardt, U., Chen, Q., et al. (2021). The contribution of global aviation to anthropogenic climate forcing for 2000 to 2018. *Atmospheric Environment*, *244*, 117834. https://doi.org/10.1016/j.atmosenv.2020.117834

Le Quéré, C., Jackson, R. B., Jones, M. W., Smith, A. J. P., Abernethy, S., Andrew, R. M., et al. (2020). Temporary reduction in daily global CO_2 emissions during the COVID-19 forced confinement. *Nature Climate Change*, *10*(7), 647–653. https://doi.org/10.1038/s41558-020-0797-x

Mahrt, F., Kilchhofer, K., Marcolli, C., Grönquist, P., David, R. O., Rösch, M., et al. (2019). The impact of cloud processing on the ice nucleation abilities of soot particles at cirrus temperatures. *Journal of Geophysical Research: Atmospheres*.

Mahrt, F., Kilchhofer, K., Marcolli, C., Grönquist, P., David, R. O., Rösch, M., et al. (2020). The impact of cloud processing on the ice nucleation abilities of soot particles at cirrus temperatures. *Journal of Geophysical Research: Atmospheres*, *125*(3). https://doi.org/10.1029/2019jd030922

Mitchell, D. L., Garnier, A., Pelon, J., & Erfani, E. (2018). CALIPSO (IIR-CALIOP) retrievals of cirrus cloud ice-particle concentrations. *Atmospheric Chemistry and Physics*, *18*(23), 17325–17354.

Mohler, O., Buttner, S., Linke, C., Schnaiter, M., Saathoff, H., Stetzer, O., et al. (2005). Effect of sulfuric acid coating on heterogeneous ice nucleation by soot aerosol particles. *Journal of Geophysical Research: Atmospheres*, *110*(D11). https://doi.org/10.1029/2004jd005169

Moore, R. H., Thornhill, K. L., Weinzierl, B., Sauer, D., D'Ascoli, E., Kim, J., et al. (2017). Biofuel blending reduces particle emissions from aircraft engines at cruise conditions. *Nature*, *543*(7645), 411–415. Retrieved from https://www.ncbi.nlm.nih.gov/pubmed/28300096

Penner, J. E., Zhou, C., Garnier, A., & Mitchell, D. L. (2018). Anthropogenic aerosol indirect effects in cirrus clouds. *Journal of Geophysical Research: Atmospheres*, *123*(20), 11652–11677. https://doi.org/10.1029/2018jd029204

Phillips, C. A., Caldas, A., Cleetus, R., Dahl, K. A., Declet-Barreto, J., Licker, R., et al. (2020). Compound climate risks in the COVID-19 pandemic. *Nature Climate Change*, *10*(7), 586–588. https://doi.org/10.1038/s41558-020-0804-2

Richardson, M. S., DeMott, P. J., Kreidenweis, S. M., Cziczo, D. J., Dunlea, E. J., Jimenez, J. L., et al. (2007). Measurements of heterogeneous ice nuclei in the Western United States in springtime and their relation to aerosol characteristics. *Journal of Geophysical Research: Atmospheres*, *112*(D2). https://doi.org/10.1029/2006jd007500

SABRE. (2020). *Market intelligence global demand data*. Retrieved from http://www.sabreairlinesolutions.com/home/software_solutions/airports/

Samset, B. H., Myhre, G., Herber, A., Kondo, Y., Li, S. M., Moteki, N., et al. (2014). Modelled black carbon radiative forcing and atmospheric lifetime in AeroCom Phase II constrained by aircraft observations. *Atmospheric Chemistry and Physics*, *14*(22), 12465–12477. https://doi.org/10.5194/acp-14-12465-2014

Schumann, U., Poll, I., Teoh, R., Koelle, R., Spinielli, E., Molloy, J., et al. (2021). Air traffic and contrail changes over Europe during COVID-19: A model study. *Atmospheric Chemistry and Physics*, *21*(10), 7429–7450.

Sourdeval, O., Gryspeerdt, E., Kraemer, M., Goren, T., Delanoe, J., Afchine, A., et al. (2018). Ice crystal number concentration estimates from lidar-radar satellite remote sensing–Part 1: Method and evaluation. *Atmospheric Chemistry and Physics*, *18*(19), 14327–14350.

Ström, J., & Ohlsson, S. (1998). In situ measurements of enhanced crystal number densities in cirrus clouds caused by aircraft exhaust. *Journal of Geophysical Research: Atmospheres*, *103*(D10), 11355–11361. https://doi.org/10.1029/98jd00807

Tesche, M., Achtert, P., Glantz, P., & Noone, K. J. (2016). Aviation effects on already-existing cirrus clouds. *Nature Communications*, *7*, 12016. https://doi.org/10.1038/ncomms12016

Urbanek, B., Groß, S., Wirth, M., Rolf, C., Krämer, M., & Voigt, C. (2018). High depolarization ratios of naturally occurring cirrus clouds near air traffic regions over Europe. *Geophysical Research Letters*, *45*(23), 13166–13172. https://doi.org/10.1029/2018gl079345

Venter, Z. S., Aunan, K., Chowdhury, S., & Lelieveld, J. (2020). COVID-19 lockdowns cause global air pollution declines. *Proceedings of the National Academy of Sciences of the United States of America*, *117*(32), 18984–18990. Retrieved from https://www.ncbi.nlm.nih.gov/pubmed/32723816

Wang, B., Lambe, A. T., Massoli, P., Onasch, T. B., Davidovits, P., Worsnop, D. R., & Knopf, D. A. (2012). The deposition ice nucleation and immersion freezing potential of amorphous secondary organic aerosol: Pathways for ice and mixed-phase cloud formation. *Journal of Geophysical Research: Atmospheres*, *117*(D16). https://doi.org/10.1029/2012jd018063

Wilkerson, J. T., Jacobson, M. Z., Malwitz, A., Balasubramanian, S., Wayson, R., Fleming, G., et al. (2010). Analysis of emission data from global commercial aviation: 2004 and 2006. *Atmospheric Chemistry and Physics*, *10*(13), 6391–6408.

Worldometers (2021). *Coronavirus cases*. Accessed on 25. 10. 2021. Retrieved from https://www.worldometers.info/coronavirus/

Yang, Y., Ren, L., Li, H., Wang, H., Wang, P., Chen, L., et al. (2020). Fast climate responses to aerosol emission reductions during the COVID-19 pandemic. *Geophysical Research Letters*, *47*(19). https://doi.org/10.1029/2020gl089788

Zhao, B., Wang, Y., Gu, Y., Liou, K. N., Jiang, J. H., Fan, J., et al. (2019). Ice nucleation by aerosols from anthropogenic pollution. *Nature Geoscience*, *12*, 602–607. https://doi.org/10.1038/s41561-019-0389-4

Zheng, B., Zhang, Q., Geng, G., Chen, C., Shi, Q., Cui, M., et al. (2021). Changes in China's anthropogenic emissions and air quality during the COVID-19 pandemic in 2020. *Earth System Science Data*, *13*(6), 2895–2907. https://doi.org/10.5194/essd-13-2895-2021

Zhou, C., & Penner, J. E. (2014). Aircraft soot indirect effect on large-scale cirrus clouds: Is the indirect forcing by aircraft soot positive or negative? *Journal of Geophysical Research: Atmospheres*, *119*(19), 11303–11320.

Zhu, J., & Penner, J. E. (2019). Global modeling of secondary organic aerosol with organic nucleation. *Journal of Geophysical Research: Atmospheres*, *124*(14), 8260–8286. https://doi.org/10.1029/2019jd030414

Zhu, J., & Penner, J. E. (2020a). Indirect Effects of Secondary Organic Aerosol on Cirrus Clouds. *Journal of Geophysical Research: Atmospheres*, *125*(7). https://doi.org/10.1029/2019jd032233

Zhu, J., & Penner, J. E. (2020b). Radiative forcing of anthropogenic aerosols on cirrus clouds using a hybrid ice nucleation scheme. *Atmospheric Chemistry and Physics*, *20*(13), 7801–7827. https://doi.org/10.5194/acp-20-7801-2020

Zhu, J., Penner, J. E., Lin, G., Zhou, C., Xu, L., & Zhuang, B. (2017). Mechanism of SOA formation determines magnitude of radiative effects. *Proceedings of the National Academy of Sciences of the United States of America*, *114*(48), 12685–12690. Retrieved from https://www.ncbi.nlm.nih.gov/pubmed/29133426

Zhu, J., Penner, J. E., Yu, F., Sillman, S., Andreae, M. O., & Coe, H. (2019). Decrease in radiative forcing by organic aerosol nucleation, climate, and land use change. *Nature Communications*, *10*(1), 423. https://doi.org/10.1038/s41467-019-08407-7